**Atmospheric
Measurement
Techniques**
Discussions

Stratospheric aerosol particle size information in Odin-OSIRIS limb scatter spectra

L. A. Rieger, A. E. Bourassa, and D. A. Degenstein

Institute of Space and Atmospheric Studies, University of Saskatchewan, Saskatchewan, Canada

Correspondence to: L. A. Rieger (landon.rieger@usask.ca)

Discussion Paper | Discussion Paper | Discussion Paper | Discussion Paper |

AMTD
6, 5065–5099, 2013

OSIRIS particle size
L. A. Rieger et al.

Title Page
Abstract | Introduction
Conclusions | References
Tables | Figures
|◄ | ►|
◄ | ►
Back | Close
Full Screen / Esc
Printer-friendly Version
Interactive Discussion

Title Page

Abstract | Introduction

Conclusions | References

Tables | Figures

◄ | ►

◄ | ►

Back | Close

Full Screen / Esc

Printer-friendly Version

Interactive Discussion

Abstract

The Optical Spectrograph and InfraRed Imaging System (OSIRIS) on-board the Odin satellite has now taken over a decade of limb scatter measurements that have been used to retrieve the Version 5 stratospheric aerosol extinction product. This product is
5 retrieved using a representative particle size distribution to calculate scattering cross sections and scattering phase functions for the forward model calculations. In this work the information content of OSIRIS measurements with respect to stratospheric aerosol is systematically examined for the purpose of retrieving particle size information along with the extinction coefficient. The benefit of using measurements at different wave-
10 lengths and scattering angles in the retrieval is studied and it is found that incorporation of the 1530 nm radiance measurement is key for a robust retrieval of particle size information. It is also found that using OSIRIS measurements at different solar geometries simultaneously provides little additional benefit. Based on these results, an improved aerosol retrieval algorithm is developed that couples the retrieval of aerosol extinction
15 and mode radius of a log-normal particle size distribution. Comparison of these results with coincident measurements from SAGE III show agreement in retrieved extinction to within approximately 10 % over the bulk of the aerosol layer, which is comparable to Version 5. The retrieved particle size, when converted to Ångström coefficient, shows good qualitative agreement with SAGE II measurements made at somewhat shorter
20 wavelengths.

1 Introduction

Stratospheric aerosols play an important role in Earth's radiative balance and have been studied using numerous instruments. The Stratospheric Aerosol and Gas Experiment (SAGE) II, in particular, operated from 1984 to 2005, and has provided an
25 invaluable record of high quality, stable, global, long term aerosol levels. This is in part due to the nature of occultation measurements, which provide an inherent calibration

through measurement of the exo-atmospheric solar spectrum as well as direct mea-
surements of atmospheric optical depth, which are relatively easy to convert to aerosol
extinction. While these occultation measurements provide distinct advantages in terms
of measurement simplicity, the technique also limits coverage, typically producing two
measurements per orbit. Measurements of limb scattered sunlight have also been used
to retrieve stratospheric aerosol extinction profiles. This technique aims to improve the
global coverage while still providing relatively good vertical resolution. Satellite limb
scatter instruments include the Optical Spectrograph and InfraRed Imaging System
(OSIRIS) (Llewellyn et al., 2004), SAGE III (Rault, 2005; Rault and Loughman, 2007)
and the SCanning Imaging Absorption spectroMeter for Atmospheric CartograpHY
(SCIAMACHY) (Bovensmann et al., 1999).

These limb scatter instruments measure vertical profiles of integrated line of sight
radiance, typically at a wide range of wavelengths from the UV to the near infrared.
As mentioned, this allows for the opportunity to measure any sunlit portion of globe,
greatly improving coverage. The cost of these measurements comes in the increased
complexity. Light that has been scattered multiple times must be accounted for, requir-
ing complex forward model calculations to perform retrievals. This is particularly difficult
for aerosols due to the signal dependence on microphysical properties in addition to
particle number density, and requires the assumption or retrieval of aerosol parameters
in addition to extinction coefficient.

This work focuses on measurements made by the OSIRIS instrument, which was
launched in February 2001, on-board the Odin satellite and continues full operation to
the time of writing. Odin is in a polar, sun-synchronous orbit with an inclination of 98°.
OSIRIS views in the orbital plane and this provides measurements from 82° S to 82° N
with equatorial crossings at 18:00 LT and 06:00 LT for the north and southbound cross-
ings, respectively. This dusk/dawn orbit provides coverage of a large latitude range. As
Odin orbits the satellite nods to scan the instrument line of sight vertically at tangent
heights from the upper troposphere to the mesosphere.

OSIRIS particle size

L. A. Rieger et al.

Title Page

Abstract | Introduction

Conclusions | References

Tables | Figures

◄ | ►

◄ | ►

Back | Close

Full Screen / Esc

Printer-friendly Version

Interactive Discussion

The Optical Spectrograph (OS) measures wavelengths from 274 to 810 nm with 1 nm resolution along a single line of sight, with a vertical sampling rate of 2 km and vertical resolution of approximately 1 km. As Odin is scanned this provides vertical information from approximately 7 to 65 km during normal aeronomy operations. The InfraRed Imager (IRI) is composed of three vertical photodiode arrays, each with 128 pixels, with filters on each channel of 1260, 1270 and 1530 nm. The measurement technique of the IRI is fundamentally different than that of the OS; each pixel measures a line of sight at a particular altitude, creating an entire vertical profile spanning tangent heights over approximately 100 km with each exposure. As the satellite nods, the imaged altitude range is then shifted.

A stratospheric aerosol retrieval was developed for use with the OSIRIS measurements by Bourassa et al. (2007). This algorithm uses a spectral ratio as the retrieval vector and the SASKTRAN forward model for radiative transfer calculations (Bourassa et al., 2008b). Scattering cross sections and phase functions used in the radiative transfer model are calculated from an assumed representative particle size distribution. The inversion is performed using the Multiplicative Algebraic Relaxation Technique, which has also been implemented in the successful retrieval of ozone (Degenstein et al., 2009) and nitrogen dioxide (Bourassa et al., 2011a) from the OSIRIS measurements. Further improvements to the aerosol algorithm, including a more sensitive aerosol measurement vector and coupled albedo retrieval, were implemented in the Version 5 algorithm and are discussed in detail by Bourassa et al. (2011b). Herein a brief overview of the Version 5 algorithm is given, and the systematic effects of the assumed particle size distribution are discussed. In Sect. 3, the sensitivity and information content of OSIRIS measurements in relation to particle size is explored to provide a foundation for an improved retrieval. Section 4 provides a development of this improved retrieval, which couples the aerosol extinction retrieval and retrieval of a particle size parameter. Here the retrieval sensitivity and error is also examined. In Sect. 5 the improved algorithm is applied to the OSIRIS data for the full mission time series and results are compared

OSIRIS particle size

L. A. Rieger et al.

Title Page

Abstract	Introduction
Conclusions	References
Tables	Figures

◀◀   ▶▶

◀   ▶

Back   Close

Full Screen / Esc

Printer-friendly Version

Interactive Discussion

against Version 5 as well as SAGE II and III measurements. Finally, conclusions are discussed in Sect. 6.

2 Version 5 algorithm

The stratospheric aerosol extinction coefficient at 750 nm, which is currently retrieved as part of the standard OSIRIS data processing, uses an assumed uni-modal log-normal particle size distribution of the form:

$$\frac{\mathrm{d}n(r)}{\mathrm{d}r} = \frac{n_{\text{aer}}}{r \ln(\sigma_g)\sqrt{2\pi}} \exp\left(-\frac{(\ln r - \ln r_g)^2}{2\ln(\sigma_g)^2}\right). \tag{1}$$

This provides a distribution with a single peak (or mode) where the number of particles is normally distributed according to the logarithm of particle radius. Aerosol concentration is then fully described by three parameters: mode radius, r_g, mode width, σ_g, and the total number of particles, n_{aer}, for each mode. For the Version 5 algorithm, a uni-modal distribution with a mode radius of 80 nm and mode width of 1.6 is assumed, as these are typical of the background aerosol loading conditions (Deshler et al., 2003). The scattering cross sections and phase functions are then calculated using Mie theory, and aerosol number density is retrieved using a single measurement vector based on the ratio of spectral radiances at two wavelengths

$$\widetilde{I}(j) = \frac{I(j, 750\,\text{nm})}{I(j, 470\,\text{nm})} \tag{2}$$

where j denotes the tangent altitude index. This normalization is used to reduce the effect of local density fluctuations in the neutral background, that would otherwise be fit with the aerosol concentration, and to increase sensitivity to the Mie scattering signal (Bourassa et al., 2007). To further increase the sensitivity to aerosol the measurement

is normalized by a modeled Rayleigh signal, $\widetilde{I}_{Ray}(j)$, yielding

$$y_j = \ln \left(\frac{\widetilde{I}(j)}{\widetilde{I}_{Ray}(j)} \right). \tag{3}$$

Finally, the measurement vector is normalized by one or more high altitude measurements. This eliminates the need for an absolute calibration and decreases the sensitivity to unknown surface albedo and tropospheric clouds (von Savigny et al., 2003). To improve the signal to noise of normalizing by a single high altitude measurement, normalization is chosen over an altitude range such that Eq. (3) is at a minimum within a chosen noise margin (Bourassa et al., 2011b). This provides the final aerosol measurement vector

$$y_j = \ln \left(\frac{\widetilde{I}(j)}{\widetilde{I}_{Ray}(j)} \right) - \frac{1}{N} \sum_{j=m}^{m+N} \ln \left(\frac{\widetilde{I}(j)}{\widetilde{I}_{Ray}(j)} \right), \tag{4}$$

where N tangent altitudes between m and $m+N$ have been used for the normalization.

Using radiance measurements in the normalization range the 750 nm albedo is retrieved assuming a Lambertian surface and by iteratively matching the measured and modeled radiances. The aerosol extinction, $\widehat{x}$ is then updated using the multiplicative algebraic reconstruction:

$$\widehat{x}_i^{(n+1)} = \widehat{x}_i^{(n)} \sum_j \frac{y_j^{obs}}{y_j^{mod}} W_{ij}. \tag{5}$$

Here the weighting matrix, $\mathbf{W}$, provides the contribution of various lines of sight at tangent altitudes, j, to the retrieved altitude, i, based on relative path lengths of the line of sight through the spherical shells. Further detail on the MART method and the determination of the weighting factors, W_{ij}, are provided in Bourassa et al. (2007, 2011b)

OSIRIS particle size

L. A. Rieger et al.

Discussion Paper | Discussion Paper | Discussion Paper | Discussion Paper

and Degenstein et al. (2004, 2009). Although the albedo is retrieved prior to aerosol extinction it is sensitive to the aerosol loading and is retrieved again after the aerosol retrieval has converged. Aerosol is then retrieved again with the updated albedo value.

The limitation of this approach is that the measurement vector, y, is dependent upon the aerosol phase function, which is dictated by the assumed particle size. Any bias in the assumed phase function is translated to the retrieved extinction. The effect of this can be tested by comparing data taken at similar locations and times, but with different viewing geometries. If the particle size, and thus the phase function is correct, then measurements will be independent of the solar scattering angle and match to within atmospheric variability. If, on the other hand, particle size has been incorrectly assumed, this will be reflected in the phase function, and the retrieval will compensate with differing amounts of aerosol depending upon the on solar scattering angle. It is possible to test this dependence through the comparison of retrievals at similar locations and times, but with different solar scattering angles. An example of two such measurements that occur for OSIRIS, one on the ascending track of the orbit and a second on the descending track is shown in Fig. 1. The crossing point of the two tracks occurs 12 h apart and, in the tropics, with scattering angles that differ by up to 60°, depending upon the season.

A comparison of ascending and descending track measurements using weekly averages for 20° N to 20° S is shown in Fig. 2. The ascending and descending node scattering angles are shown in the top panel, and the weekly aerosol extinction ratios averaged between 25 and 28 km are shown in the bottom panel for the respective orbital tracks. Extinction ratio is the ratio of extinction due to aerosol to the molecular extinction and is analogous to volume mixing ratio. A systematic difference between the measurements is apparent and correlates well with the difference in scattering angles, indicating that the phase function and assumed particle size distribution are likely incorrect. After 2006, the local time of the ascending node increases past that of local sunset due to orbital precession and the tangent point is no longer sunlit. This represents the

Title Page

Abstract | Introduction

Conclusions | References

Tables | Figures

Back | Close

Full Screen / Esc

Printer-friendly Version

Interactive Discussion

worst case for OSIRIS and lower altitudes and mid to high latitudes do not show this bias to nearly this degree.

Removal of this bias requires more accurate estimation of the particle size parameters used in the SASKTRAN model, and the following section discusses the information available from OSIRIS to retrieve particle size directly.

3 OSIRIS information content

In Version 5 the normalization of the 750 nm radiance by the radiance at 470 nm was beneficial in minimizing the effect of uncertainty in the local air density. However, the 470 nm measurements are not completely insensitive to aerosol, particularly smaller particles, and for the purposes of retrieving particle size information this spectral normalization creates a more non-linear solution space and greatly increases the difficulty of the retrieval. Therefore, in this work the 470 nm normalization is removed from the aerosol measurement vector. The single wavelength measurement vector is then:

$$y_j = \ln\left(\frac{I(j,\lambda)}{I_{\text{Ray}}(j,\lambda)}\right) - \frac{1}{N}\sum_{j=m}^{m+N}\ln\left(\frac{I(j,\lambda)}{I_{\text{Ray}}(j,\lambda)}\right). \qquad (6)$$

Note here that for a given wavelength this is similar to Eq. (6), except that $\widetilde{I}(j,\lambda)$ has been replaced with the un-normalized $I(j,\lambda)$. We now explore the particle size information contained in measurement vectors of this type for the full set of wavelengths measured by OSIRIS.

To extract particle size information from the wavelength dependence of OSIRIS measurement vectors, the wavelength dependence of the measurement vector due to changing particle size must be considerably larger than the measurement noise. This dependence is explored by simulating the aerosol measurement vector for multiple wavelengths and particle sizes. This was done by assuming three different size distributions and extinctions which produce the same 750 nm measurement vector;

that is, three atmospheric states which are essentially indistinguishable with a single wavelength retrieval at 750 nm. The first is a bi-modal distribution, the second is a "fine mode" distribution, used in the Version 5 retrievals and corresponding to a typical background state, and the third is a single mode "representative" distribution with the same
5   effective radius as the bi-modal distribution. The resulting aerosol measurement vectors were then modeled at a range of wavelengths for an OSIRIS scan with a scattering angle of 60° and solar zenith angle of 79°. The change of the measurement vector for the three cases then indicates the sensitivity to particle size. Figure 3 shows that the measurement vectors below approximately 800 nm provide almost no discrimination
10   between particle sizes, and thus little to no additional information that could be used for particle size retrieval. However, measurement vectors at longer wavelengths begin to diverge; by up to 40 % at 1500 nm for the case studied here. While this precludes retrieving particle size with the Optical Spectrograph (OS) measurements alone, which only go up to 800 nm, a measurement near the long-wavelength end of the OS mea-
15   surements, say at 750 nm, can be combined with measurements from the infrared imager for retrieval of particle size information. The imager channels at 1260 and 1270 nm were designed to measure excited state oxygen emission and this emission renders these channels unusable for aerosol retrieval; however, the 1530 nm channel, which was designed to measure an excited OH emission that is extremely weak during day-
20   time, can be used for the aerosol retrieval. A proof-of-concept of particle size retrieval using a combination of OSIRIS spectral measurements is presented in Bourassa et al. (2008a); here we systematically explore the full potential of the particle size information in the OSIRIS measurements and compare these new results with the SAGE II and III measurements.
25   In addition to the spectral dependence, Fig. 2 shows that there is a solar scattering angle, or viewing geometry, dependence on particle size. However, these pieces of information are not independent, and the ability to derive multiple pieces of information depends on both the orthogonality of the measurement vectors and the instrument noise. Twomey (1977) developed a method of determining information content

of a measurement set based on the orthogonality of the measurement kernels. This technique was employed by Thomason and Poole (1992); Thomason et al. (1997) in determining particle size properties from the SAGE II data. This method relies on the ability to write the measurement vector, $\boldsymbol{y}$, as an integration over the particle distribu-

5   tion, dV/dr such as

$$y_k = \int_0^\infty K_k(r)\frac{dV(r)}{dr}dr. \tag{7}$$

where $K(r)$, is the kernel describing the sensitivity of the measurement to particles of size r. For occultation measurements this formulation is accurate due to the fact that the measurements are linear – addition of a particle of size r, does not affect the shape

10   of the kernel, $K(r)$. This is not strictly true in limb measurements due to the effects of multiple scattering. Adding a particle of radius r will affect the amount of light that is scattered by other aerosol particles, changing $K(r)$ for all r. The applicability of this technique to OSIRIS measurements is then limited by the amount of aerosol-to-aerosol multiple scatter, and as this term increases Eq. (7) becomes increasingly inaccurate.

15   As a starting point, we assume an optically thin, single scatter atmosphere. In this case the aerosol measurement vector is proportional to the triple product of number density, scattering cross section, σ_{aer}, and the phase function, p, at the tangent point. The kernel, at wavelength k, is then

$$K_k(r) = \frac{3}{4\pi r^3}\sigma_{aer}(\lambda_k, r)p(\Theta_k, \lambda_k, r)\Delta s, \tag{8}$$

20   where σ_{aer} is the aerosol scattering cross section, p is the phase function, and Δs is the path length through the tangent point shell. A more accurate kernel which includes multiple scatter terms as well as path length integration can be computed using SASKTRAN by modeling the measurement vector for a variety of mono-disperse particles with a constant aerosol volume density. These will depend slightly on the

aerosol profile chosen due to the path length integration and multiple scattering, how-
ever for stratospheric altitudes and low aerosol loadings the effect is minimal. This was
done for a matched pair of scans with solar zenith angles of 89° and 83° and solar
scattering angles of 60° (forward scattering) and 118° (back scattering) respectively.
Kernels for these geometries at 750 and 1530 nm are shown in Fig. 4. The 750 nm
measurements are more sensitive to smaller particles, with the backscatter geome-
tries having a broader response. The single scatter kernels computed from Eq. (8) are
also included for comparison. Although calculation of multiple scattering terms tends to
smooth the sensitivity across particle size, the single scatter approximation is still quite
good despite the sweeping assumptions. This indicates that the magnitude and shape
of a specific aerosol profile chosen for modeling the multiple scatter kernels is not cru-
cial when examining measurement sensitivities and information content provided that
aerosol extinction remains somewhat low. These kernels also show that the OSIRIS
limb measurements are most sensitive to particles in the 100 nm to few micron range.

The amount of aerosol information obtainable from the measurements then depends
on the difference in sensitivity to various particle sizes. From Fig. 4 we can see that
while the shape of each kernel is different, there is significant overlap of sensitivity, par-
ticularly to particles in the few hundred nanometer size range. Extracting information
from measurements that have significant overlap can be difficult and require unreal-
istically high signal to noise ratios. It is, however, possible to assess the information
content of a noisy measurement set based on the kernels using eigenvector analy-
sis explored by Twomey (1977). In this analysis a measurement can be thought of as
containing information if it cannot be predicted within error from other measurements.
Predicting a measurement is possible if the kernel can be written as a linear combina-
tion of other kernels,

$$K_k(r) = -a_k^{-1} \sum_{l \neq k} a_l K_l(r), \tag{9}$$

where, $K_k(r)$ is the predicted kernel as a function of particle radius. This is strictly true only if the kth eigenvalue, L_{kk}, of the covariance matrix, $\mathbf{KK}^\mathsf{T}$ is zero. However, if the eigenvalue is sufficiently small, then the measurement can be predicted within error. The number of independent measurements is then determined by the number of eigenvalues which exceed the threshold

$$\frac{L_{kk}}{L_{\max}} \gg \epsilon^2. \tag{10}$$

Where ϵ is the relative measurement error. For the kernels shown in Fig. 4 the normalized eigenvalues are:

$$1.000, \quad 0.0807, \quad 0.0425, \quad 0.0144. \tag{11}$$

This translates to three pieces of information if the relative error in the measurements is better than 20 % and four pieces if the error is better than 10 %. Although up to four pieces of information are present, this does not guarantee the retrieval of the three desired quantities relating to the aerosol particle size distribution (number density, mode radius and mode width) due to the shape of the kernels being unable to accurately reproduce an arbitrary log-normal distribution. Additionally, relying on multiple geometries introduces several limitations, namely retrievals are only possible where matching pairs exist and where the separation in scattering angle is large. For these reasons we have chosen to use only one geometry per retrieval incorporating two wavelengths, one at 750 nm and a second at 1530 nm. This allows for one additional piece of particle size information to be retrieved on a scan-by-scan basis.

4 Coupled extinction and particle size retrieval

To utilize the two pieces of information we maintain the assumption of a uni-modal log-normal distribution with a mode width of 1.6 and attempt to retrieve mode radius

OSIRIS particle size

L. A. Rieger et al.

and extinction using measurement vectors at 750 and 1530 nm as defined in Eq. (6). At each iteration the mode radius and extinction are updated at each tangent altitude using the Levenberg–Marquardt algorithm (Marquardt, 1963),

$$\left(\mathbf{K}_j^\mathsf{T}\mathbf{K}_j + \gamma \mathrm{diag}(\mathbf{K}_j^\mathsf{T}\mathbf{K}_j)\right)\boldsymbol{\delta}_j = \mathbf{K}_j^\mathsf{T}\left(\mathbf{y}_j^{\mathrm{mod}} - \mathbf{y}_j^{\mathrm{obs}}\right) \tag{12}$$

where $\mathbf{K}_j$ is the Jacobian at altitude j,

$$\mathbf{K}_j = \begin{pmatrix} \dfrac{\partial y_j(750\,\mathrm{nm})}{\partial r_g} & \dfrac{\partial y_j(750\,\mathrm{nm})}{\partial n_{\mathrm{aer}}} \\ \dfrac{\partial y_j(1.53\,\mu\mathrm{m})}{\partial r_g} & \dfrac{\partial y_j(1.53\,\mu\mathrm{m})}{\partial n_{\mathrm{aer}}} \end{pmatrix}. \tag{13}$$

The atmospheric state is then updated using

$$\widehat{\mathbf{x}}_j^{(n+1)} = \widehat{\mathbf{x}}_j^{(n)} + \boldsymbol{\delta}_j. \tag{14}$$

To improve computation time of the Jacobian the entire aerosol profile is shifted and the forward difference method is used to compute the element at each altitude. This neglects the effects of altitude coupling, however convergence is still typically achieved in 10 iterations. The convergence limits are given in Table 1, and convergence is satisfied if any of the limits are met for all retrieved altitudes.

The error in the retrieved quantities can be estimated from the error analysis developed by Rodgers (2000), which is broken into forward model error, measurement error, and smoothing error. These are discussed in detail in the following section and the error is simulated for a typical scan.

4.1 Measurement error

The measurement error can be broken into two components, a random error, $\delta \mathbf{y}_\mathrm{R}$, due to the measurement noise that is uncorrelated between altitudes and a systematic

error, δy_{S_k}, due to the high altitude calibration that is entirely correlated between altitudes. The random error in the measurement vector $\boldsymbol{y}_k$ at altitude j can be determined from error in the spectral radiance measurement as

$$\delta y_{R_{kj}} = \frac{\delta I_j(\lambda_k)}{I_j(\lambda_k)}. \tag{15}$$

5 Since the high altitude normalization results in a shift of the measurement vector based on the spectral radiance measurements at high altitudes, the systematic error is the same for all altitudes and given by

$$\delta y_{S_k} = \frac{1}{N} \sqrt{\sum_{j=m}^{m+N} \frac{\delta I_j^2(\lambda_k)}{I_j^2(\lambda_k)}}. \tag{16}$$

10 Following the error analysis by Barlow (1989) the random and systematic errors are independent and thus the total variance of a measurement vector at altitude j is simply the quadrature sum of both errors

$$\delta y_{kj}^2 = \delta y_{R_{kj}}^2 + \delta y_{S_k}^2. \tag{17}$$

The covariance of the errors can be found similarly, however the random errors will cancel, leaving only the squared systematic terms. The error covariance matrix, $\mathbf{S}_\epsilon$, for 15 wavelength k is then

$$\mathbf{S}_{\epsilon_k} = \begin{pmatrix} \delta y_{R_{k1}}^2 + \delta y_{S_k}^2 & \cdots & \delta y_{S_k}^2 \\ \vdots & \ddots & \vdots \\ \delta y_{S_k}^2 & \cdots & \delta y_{R_{kj}}^2 + \delta y_{S_k}^2 \end{pmatrix}. \tag{18}$$

The measurement error for the optical spectrograph and infrared imager is quite different due to the measurement techniques. As the optical spectrograph is scanned

vertically the exposure time can be increased, resulting in approximately the same number of photons being counted with each exposure; resulting in noise that increases only slightly with altitude, ranging from approximately 0.5–1 % of the total signal. The IR channels image the entire vertical profile simultaneously, resulting in considerable noise at higher altitudes, typically on the order of 10 %. Fortunately, the imager takes multiple profiles for each optical spectrograph scan, often 30 or more, which can be collapsed into an average profile to reduce the noise. Despite this averaging, error in the infrared channel still exceeds that of the optical spectrograph. This produces a measurement vector error of approximately 5 % in infrared and 1 % at 750 nm. In the retrieved quantities this translates to an error of 10 % in the retrieved quantities near the peak of the aerosol layer.

4.2 Smoothing error

The averaging kernel matrices for the extinction and mode radius quantities are shown in Fig. 5. These are calculated numerically by perturbation of a typical aerosol extinction and mode radius profile at each altitude and successive retrieval using simulated radiances for each state. The averaging kernel for extinction is very nearly unity for 10 km and above with very little smoothing of the profile, as was seen in the Version 5 algorithm. The resulting smoothing error in extinction is typically less than 5 % for most altitudes, although this increases to more than 10 % below 10 km. Changes in mode radius are not captured as accurately at altitudes below 15 km with approximately half of the change being added to the perturbed altitude. Despite the larger off diagonal elements in the mode radius averaging kernel, error for typical cases are limited to less than 10 % due to more accurate a priori estimates.

4.3 Albedo error

One of the largest uncertainties results from the unknown albedo at 1530 nm. Although the albedo is retrieved at 750 nm, the same cannot currently be done at 1530 nm due

a lack of an absolute calibration in the infrared channels. The immediate solution is to assume the 1530 nm albedo is equal to that at 750 nm. Because the error due to albedo may be large it is best to estimate the error through a simulated retrieval. To test a scenario with a large albedo contribution a scan with a scattering angle of 118° and zenith angle of 72° was simulated with an assumed 1530 nm albedo of 0.5. OSIRIS measurements were then simulated when the true albedo was 0 and 1. This produced an error of approximately 15 % in the retrieved extinction and 30 % in the retrieved mode radius. This is a near worst-case scenario however, and typical errors are expected to be less.

4.4 Total error

A scan with a forward geometry was simulated assuming a typical background aerosol loading and the relative errors due to measurement, smoothing and 1530 nm albedo are shown in Fig. 6. At altitudes above 30 km and below 15 km error begins to dominate the signal, with virtually all of the error due to measurement noise. In the bulk of the aerosol layer this error reduces to approximately 10–15 % for both retrieved quantities. The error budget is primarily due to the 1530 nm measurements, which are approximately 5–10 times noisier than the 750 nm measurements.

The retrieved error due to measurement noise is dependent upon the aerosol concentration due to the decreasing sensitivity of the measurements with increasing optical depth. To test this dependence the aerosol profile was scaled by factors of 0.02 to 3 of the typical value and the error retrieved for each case. Results are shown in Fig. 7 for several tangent altitudes. The error in extinction decreases approximately linearly with decreased aerosol loading with a noise floor of approximately 4×10^{-6} at 30 km increasing to 4×10^{-5} at 10 km. Error in retrieved mode radius is relatively constant ranging from 0.01 μm at 30 km to 0.03 μm at 10 km, provided the extinction is greater than approximately 4×10^{-5}. Although this study was chosen as a typical case several physical and measurement factors effect the retrieval error including solar scattering angle, solar zenith angle, tangent altitude, and particle size as well as the vertical distribution of aerosols. As such this study is meant to give an estimate of the error involved, but

is not comprehensive. Determination of error for additional measurements requires the application of this error analysis on a case-by-case basis.

4.5 Ångström conversion

Although mode radius for a fixed mode width is the retrieved particle size parameter, it is certainly sensitive to the true mode width and the presence of a second mode of larger particles. One option for comparing and using the retrieved particle size information is through conversion of the mode radius to the Ångström coefficient, α, which is an empirical relationship between the aerosol cross section at two wavelengths (Ångström, 1964),

$$\frac{\sigma_{\mathrm{aer}}(\lambda_1)}{\sigma_{\mathrm{aer}}(\lambda_0)} = \left(\frac{\lambda_1}{\lambda_0}\right)^{-\alpha}. \tag{19}$$

The efficacy of this conversion can be seen by simulating OSIRIS measurements when the true state violates the assumptions of the uni-modal log-normal model. For this test a true state was chosen that was largely bimodal with a fine mode with a mode radius of 90 nm and mode width of 1.75. The second, coarse mode of particles was given a mode radius of 400 nm and mode width of 1.2. The peak 750 nm aerosol extinction was set to be $7 \times 10^{-4}\,\mathrm{km}^{-1}$ with approximately half of this coming from the coarse mode. As altitude increases this fraction decreases. The retrieved aerosol was assumed to have a single mode of particles with a mode width of 1.6. Simulated retrievals were performed for 765 OSIRIS measurements with a variety of scattering and zenith angles. The mean error and standard deviation of the retrieved extinction and Ångström coefficient are shown in Fig. 8. Error in the retrieved extinction was typically 5–10 % with an error in the Ångström coefficient of 10–15 %. This shows that even under largely bimodal conditions the coupled retrieval of extinction and mode radius produce robust results with little bias and only a slight dependence on measurement geometry.

5   Results

5.1   Retrieval consistency

The error in the retrieved extinction due to particle size in the Version 5 retrievals was evident in internal comparisons between the orbital ascending and descending track measurements, as shown in Sect. 2. This analysis was repeated with results from the coupled particle size retrieval algorithm and are shown in Fig. 9. While the scattering angle dependence is clear in the Version 5 data, with substantial separation of the ascending and descending track measurements, this is no longer the case with the coupled retrieval, denoted Version 6. A strong seasonal cycle which peaks near January is still present, however this has also been measured by multiple lidars (Hofmann et al., 2009; Uchino et al., 2012). Although much of the systematic bias has been removed from this data set, each individual measurement now appears noisier. This is due to the inclusion of the 1530 nm measurements which are considerably noisier than those from the optical spectrograph.

5.2   SAGE III recomparison

In operation from 2001 until 2005, SAGE III measured aerosol extinction profiles at nine wavelengths, ranging from 385 nm to 1.54 µm. SAGE III was launched on the Meteor 3M platform into a polar orbit, performing occultations in the mid to polar latitudes. With an accuracy and precision on the order of 10 %, and a channel at 755 nm, SAGE III provides an excellent data set for comparison (Thomason et al., 2010). Bourassa et al. (2011b) compared the Version 5.07 algorithm with coincident SAGE III measurements using a coincident criteria of ±6 h, ±1° latitude and ±2.5° longitude. The average percent difference between the SAGE III and Version 5 OSIRIS measurements separated by year are shown as the solid red lines in Fig. 10; the dashed red lines show one standard deviation. In general, the agreement is quite good with an average difference typically less than 10 %. However, nearly all altitudes in 2005 show a positive bias of up

to 20 % with an increased standard deviation. This is likely explained by an inaccurate particle size assumption during the increased aerosol loading caused by the 2004 Mt. Manam eruption.

This comparison was repeated using the same coincident criteria for the Version 6 retrievals with results shown in black in Fig. 10. Generally, agreement with the SAGE III measurements is comparable between versions, with typical accuracy of 10–15 %. The standard deviation is also similar at approximately 20 % at 15 km increasing to 50 % by 30 km. Agreement is better in 2005, after the Mt. Manam eruption, however Version 6 also underestimates extinction from 25–30 km. Although these results are promising the measurements are during low levels of aerosol with minimal volcanic influence and so are not expected to be significantly different from the Version 5 results.

5.3 SAGE II comparison

SAGE II (Russell and McCormick, 1989) was launched in 1985, and continued operating until mid 2005, providing approximately three years of overlap with the OSIRIS mission. SAGE II produced high quality measurements for the duration of its lifetime with the 525 and 1020 nm channels agreeing well with SAGE III, with typical uncertainties less than 15 % for the majority of the aerosol layer (Yue et al., 2005). This overlap period also contains good tropical coverage with two volcanic eruptions: Mts. Ruang (Ru) and Reventador (Ra) in 2003, and Mt. Manam (Ma) in 2004, providing a good test of the OSIRIS particle size retrieval. Figure 11 shows the retrieved Ångström coefficients in 45 day averages from the SAGE II and OSIRIS satellites in the tropics for 2002 through 2005. In general both show an Ångström coefficient increasing with altitude. Note also the increase in the Ångström coefficients in both data sets after the Ruang/Reventador and Manam eruptions, suggesting an increase in the number of small particles.

Although large scale features agree qualitatively, OSIRIS retrieves a systematically higher Ångström coefficient, particularly at lower altitudes. Some of this discrepancy is due to the differences in wavelength between the two satellites. The longer OSIRIS

wavelengths become optically thick at lower altitudes than the shorter wavelengths, increasing sensitivity in the upper troposphere and lower stratosphere. Also, although extinction is an approximately linear function of wavelength (in log space) this is not strictly true and causes a dependency of the Ångström coefficient on the wavelengths chosen. For very small particles ($r \lesssim 100$ nm) the Ångström coefficients of both wavelength ranges approach the Rayleigh limit of four, indicating that at high altitudes, where particles are expected to be small, agreement should be better, as is the case. For moderately sized particles ($r \lesssim 1000$ nm) however, the 525/1020 nm cross section ratio is considerably smaller than that of 750/1530 nm, indicating that where larger particles are present the Ångström coefficient derived from SAGE II should be systematically smaller than those from OSIRIS. While the wavelength difference accounts for much of the discrepancy some is likely due to the particle size assumptions, including the choice of a uni-modal log-normal distribution and particular mode width. Additionally, a six month cycle is present in the OSIRIS data which is likely due to the error in the 1530 nm albedo. In the tropics the solar zenith angle varies biannually, increasing the effect of albedo error when the sun is higher in the sky.

6 Conclusions

Through incorporation of the 1530 nm infrared imager measurement, OSIRIS measurements can be used to retrieve one piece of particle size information. Although incorporation of multiple viewing geometries does add information, for OSIRIS geometries this information is minimal and comes with significant drawbacks in coverage. Using measurements at 750 and 1530 nm a retrieval algorithm was developed that couples the retrieval of extinction with the mode radius parameter of the log-normal distribution. This reduces the dependence of the retrieved extinction on the assumed aerosol microphysics. Comparison of retrieved extinctions on the ascending and descending orbital tracks show greatly reduced dependence on viewing geometry. Unfortunately, retrievals are now noisier due to the inclusion of the infrared imager measurement. Comparisons

with SAGE II show that the retrieved Ångström coefficient is physically realistic in the tropics during both volcanic and non-volcanic periods for the bulk of the stratospheric layer, although the results shows some bias due to the particle size assumptions of a log-normal distribution with a fixed mode width as well as the inability to measure the albedo at 1530 nm. A re-comparison with the SAGE III measurements shows that for mid to polar latitudes the extinction measurements are in good agreement, particularly during 2005 after the Mt. Manam eruption.

References

Ångström, A.: The parameters of atmospheric turbidity, Tellus, 16, 64–75, 1964.

Barlow, R. J.: Statistics: a Guide to the Use of Statistical Methods in the Physical Sciences, Wiley, England, 1989.

Bourassa, A. E., Degenstein, D. A., Gattinger, R. L., and Llewellyn, E. J.: Stratospheric aerosol retrieval with OSIRIS limb scatter measurements, J. Geophys. Res., 112, D10217, doi:10.1029/2006JD008079, 2007.

Bourassa, A. E., Degenstein, D. A., and Llewellyn, E. J.: Retrieval of stratospheric aerosol size information from OSIRIS limb scattered sunlight spectra, Atmos. Chem. Phys., 8, 6375–6380, doi:10.5194/acp-8-6375-2008, 2008a.

Bourassa, A. E., Degenstein, D. A., and Llewellyn, E. J.: SASKTRAN: A spherical geometry radiative transfer code for efficient estimation of limb scattered sunlight, J. Quant. Spectrosc. Ra., 109, 52–73, doi:10.1016/j.jqsrt.2007.07.007, 2008b.

Bourassa, A. E., McLinden, C. A., Sioris, C. E., Brohede, S., Bathgate, A. F., Llewellyn, E. J., and Degenstein, D. A.: Fast NO_2 retrievals from Odin-OSIRIS limb scatter measurements, Atmos. Meas. Tech., 4, 965–972, doi:10.5194/amt-4-965-2011, 2011a.

Bourassa, A. E., Rieger, L. A., Lloyd, N. D., and Degenstein, D. A.: Odin-OSIRIS stratospheric aerosol data product and SAGE III intercomparison, Atmos. Chem. Phys. Discuss., 11, 25785–25811, doi:10.5194/acpd-11-25785-2011, 2011b.

Full Screen / Esc

Printer-friendly Version

Interactive Discussion

Bovensmann, H., Burrows, J. P., Buchwitz, M., Frerick, J., Noël, S., Rozanov, V. V., Chance, K. V., and Goede, A. P. H.: SCIAMACHY: Mission Objectives and Measurement Modes, J. Atmos. Sci., 56, 127–150, 10.1175/1520-0469(1999)056$<$0127:SMOAMM$>$$2.0.CO;2, 1999.

5 Degenstein, D. A., Llewellyn, E. J., and Lloyd, N. D.: Tomographic retrieval of the oxygen infrared atmospheric band with the OSIRIS infrared imager, Can. J. Phys., 82, 501–515, 2004.

Degenstein, D. A., Bourassa, A. E., Roth, C. Z., and Llewellyn, E. J.: Limb scatter ozone retrieval from 10 to 60 km using a multiplicative algebraic reconstruction technique, Atmos. Chem. Phys., 9, 6521–6529, doi:10.5194/acp-9-6521-2009, 2009.

10 Deshler, T., Hervig, M. E., Hofmann, D. J., Rosen, J. M., and Liley, J. B.: Thirty years of in situ stratospheric aerosol size distribution measurements from Laramie, Wyoming (41° N), using balloon-borne instruments, J. Geophys. Res., 108, 4167, doi:10.1029/2002JD002514, 2003.

Hofmann, D., Barnes, J., O'Neill, M., Trudeau, M., and Neely, R.: Increase in background stratospheric aerosol observed with lidar at Mauna Loa Observatory and Boulder, Colorado, Geo-
15 phys. Res. Lett., 36, L15808, doi:10.1029/2009GL039008, 2009.

Llewellyn, E., Lloyd, N. D., Degenstein, D. A., Gattinger, R. L., Petelina, S. V., Bourassa, A. E., Wiensz, J. T., Ivanov, E. V., McDade, I. C., Solheim, B. H., McConnell, J. C., Haley, C. S., von Savigny, C., Sioris, C. E., McLinden, C. A., Griffioen, E., Kaminski, J., Evans, W. F. J., Puck-rin, E., Strong, K., Wehrle, V., Hum, R. H., Kendall, D. J. W., Matsushita, J., Murtagh, D. P.,
20 Brohede, S., Stegman, J., Witt, G., Barnes, G., Payne, W. F., Piche, L., Smith, K., War-shaw, G., Deslauniers, D. L., Marchand, P., Richardson, E. H., King, R. A., Wevers, I., McCreath, W., Kyrola, E., Oikarinen, L., Leppelmeier, G. W., Auvinen, H., Megie, G., Hauchecorne, A., Lefevre, F., de La Noe, J., Ricaud, P., Frisk, U., Sjoberg, F., von Scheele, F., and Nordh, L.: The OSIRIS instrument on the Odin spacecraft, Can. J. Phys., 82, 411–422,
25 doi:10.1139/p04-005, 2004.

Marquardt, D. W.: An algorithm for least-squares estimation of nonlinear parameters, J. Soc. Ind. Appl. Math., 11, 431–441, available at: http://www.jstor.org/stable/2098941, 1963. Last accessed: June 4, 2013.

Rault, D. F.: Ozone profile retrieval from Stratospheric Aerosol and Gas Experi-
30 ment (SAGE III) limb scatter measurements, J. Geophys. Res.-Atmos., 110, D09309, doi:10.1029/2004JD004970, 2005.

Rault, D. and Loughman, R.: Stratospheric and upper tropospheric aerosol retrieval from limb scatter signals, Proc. SPIE 6745, doi:10.1117/12.737325, 2007. 25787, 25795

OSIRIS particle size

L. A. Rieger et al.

Rodgers, C. D.: Inverse methods for atmospheric sounding: theory and practice, World Scientific, Singapore, 2000.

Russell, P. B. and McCormick, M. P.: SAGE II aerosol data validation and initial data use – an introduction and overview, J. Geophys. Res., 94, 8335–8338, doi:10.1029/JD094iD06p08335, 1989.

Thomason, L. W. and Poole, L. R.: Use of stratospheric aerosol properties as diagnostics of Antarctic vortex processes, J. Geophys. Res., 98, 23003–23012, doi:10.1029/93JD02461, 1992.

Thomason, L. W., Poole, L. R., and Deshler, T.: A global climatology of stratospheric aerosol surface area density deduced from Stratospheric Aerosol and Gas Experiment II measurements: 1984–1994, J. Geophys. Res., 102, 8967–8976, doi:10.1029/96JD02962, 1997.

Thomason, L. W., Moore, J. R., Pitts, M. C., Zawodny, J. M., and Chiou, E. W.: An evaluation of the SAGE III version 4 aerosol extinction coefficient and water vapor data products, Atmos. Chem. Phys., 10, 2159–2173, doi:10.5194/acp-10-2159-2010, 2010.

Twomey, S.: Introduction to the Mathematics of Inversion In Remote Sensing and Indiret Measurements, Elsevier Scientific Publishing Company, New York, 1977.

Uchino, O., Sakai, T., Nagai, T., Nakamae, K., Morino, I., Arai, K., Okumura, H., Takubo, S., Kawasaki, T., Mano, Y., Matsunaga, T., and Yokota, T.: On recent (2008–2012) stratospheric aerosols observed by lidar over Japan, Atmos. Chem. Phys., 12, 11975–11984, doi:10.5194/acp-12-11975-2012, 2012.

von Savigny, C., Haley, C. S., Sioris, C. E., McDade, I. C., Llewellyn, E. J., Degenstein, D., Evans, W. F. J., Gattinger, R. L., Griffioen, E., Kyrölä, E., Lloyd, N. D., McConnell, J. C., McLinden, C. A., Mégie, G., Murtagh, D. P., Solheim, B., and Strong, K.: Stratospheric ozone profiles retrieved from limb scattered sunlight radiance spectra measured by the OSIRIS instrument on the Odin satellite, Geophys. Res. Lett., 30, 1755, doi:10.1029/2002GL016401, 2003.

Yue, G. K., Lu, C.-H., and Wang, P.-H.: Comparing aerosol extinctions measured by Stratospheric Aerosol and Gas Experiment (SAGE) II and III satellite experiments in 2002 and 2003, J. Geophys. Res., 110, D11202, doi:10.1029/2004JD005421, 2005.

Title Page

Abstract | Introduction

Conclusions | References

Tables | Figures

|◄ | ►|

◄ | ►

Back | Close

Full Screen / Esc

Printer-friendly Version

Interactive Discussion

Title Page

Abstract | Introduction

Conclusions | References

Tables | Figures

Back | Close

Full Screen / Esc

Printer-friendly Version

Interactive Discussion

Table 1. Levenberg–Marquardt convergence limits.

Jacobian norm	Step size	Total residual	Iteration limit
10^{-5}	0.01 %	10^{-4}	12

Title Page

Abstract | Introduction

Conclusions | References

Tables | Figures

|◄ | ►|

◄ | ►

Back | Close

Full Screen / Esc

—— Descending Track —— Ascending Track
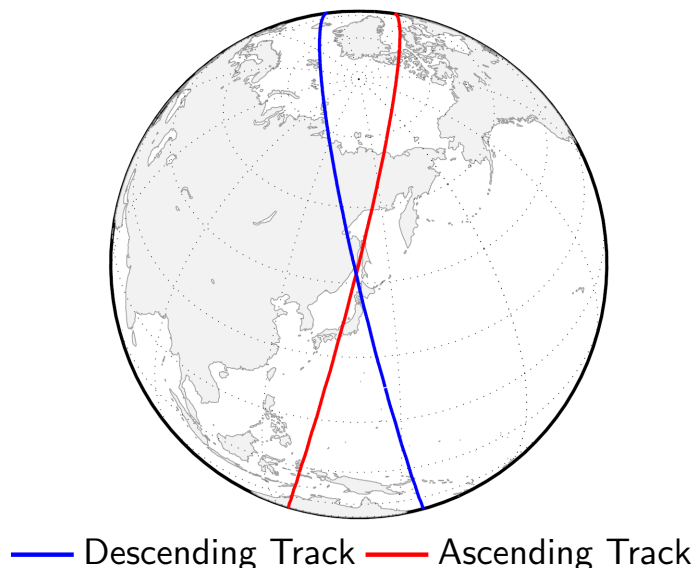
Fig. 1. OSIRIS often measures the same location twice over the course of 12 h due to orbit. Here an example of an ascending track is shown in red and a descending track in blue. The crossing point is the matched pair of scans, 11222020 and 11229004, where the same location was measured twice, approximately 12 h apart and with different viewing geometries.

● Descending Track ● Ascending Track
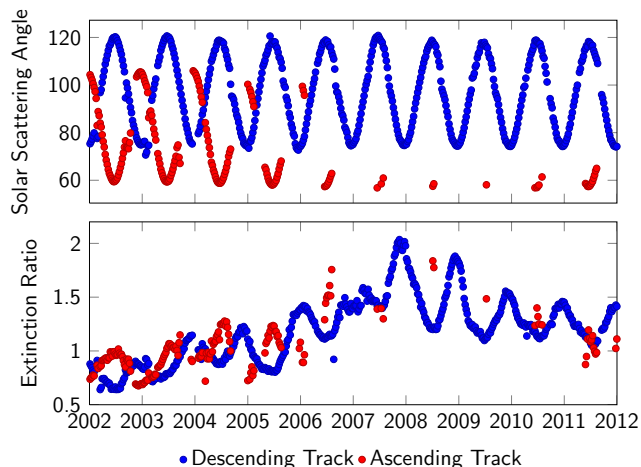
Fig. 2. The bottom panel shows the weekly averaged aerosol/molecular extinction ratio between 23 and 28 km from latitudes 20° N to 20° S split into the ascending (red) and descending track (blue) measurements. Shown in the top panel are the scattering angles for corresponding measurements. A systematic difference in the extinction ratio is apparent that depends on the difference in the scattering angles.
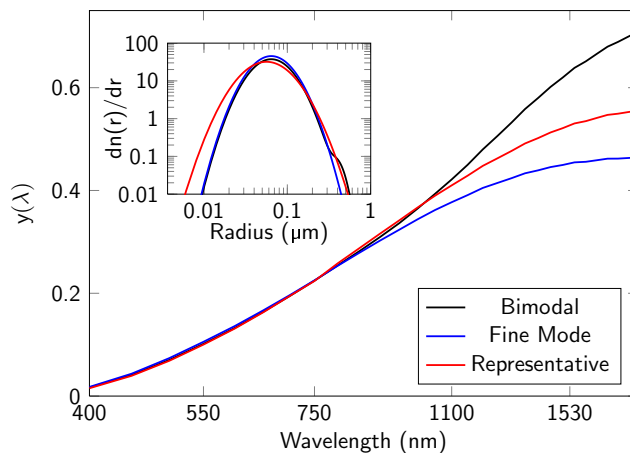
Fig. 3. Modelled sensitivity of the aerosol measurement vectors from scan 6432001 as a function of wavelength for three particle size distributions at 22.5 km. Shown in inset are the three size distributions used for the modelling.
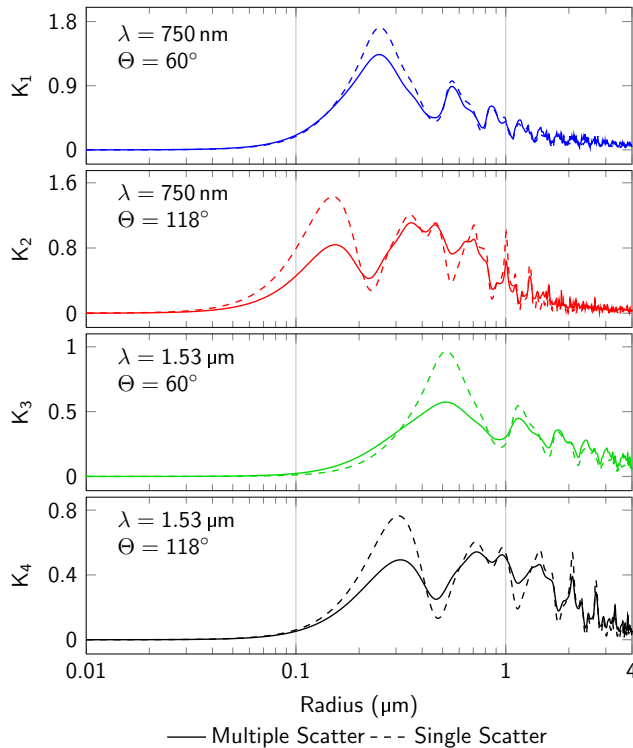
Fig. 4. Simulated measurement vector kernels for a matched pair of scans at 22.5 km for a range of mono-disperse particles with radius r. The wavelength, λ, and solar scattering angle, Θ, of each measurement vector is given in the top left of the panels. Solid lines are the kernels calculated using the multiple scattering SASKTRAN forward model, while the dashed curves show the kernels calculated from Eq. (8). Area has been normalized to one for all kernels.
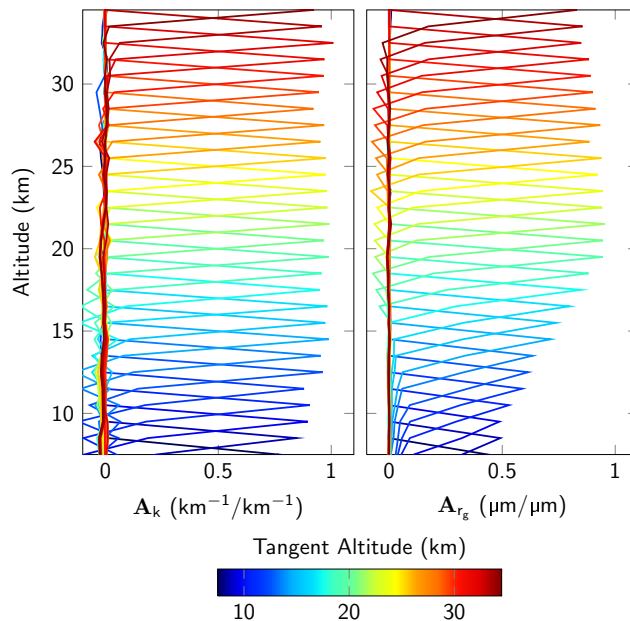
Fig. 5. Averaging kernels for the simulated extinction and mode radius retrievals using lines of sight spaced at 1 km intervals. Left panel shows the extinction averaging kernels with the mode radius averaging kernels shown on the right.
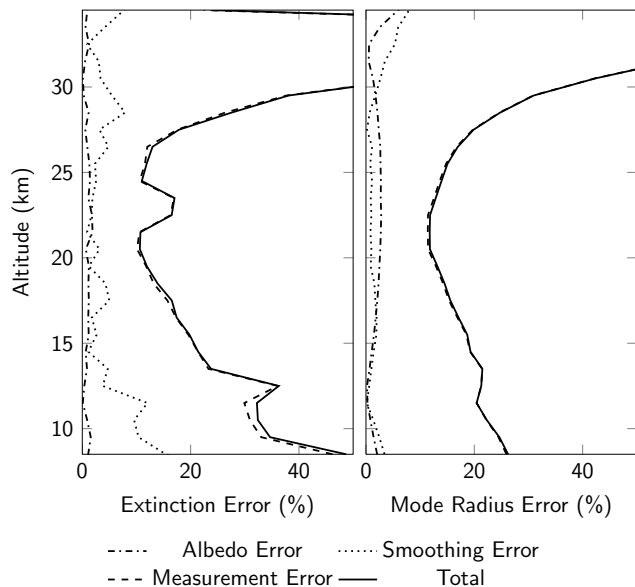
Fig. 6. Total relative error in the retrieved quantities due to albedo, smoothing and measurement error contributions for a simulated measurement with a solar scattering angle of 61° and a solar zenith angle of 89°. The aerosol profile used in the simulation was typical of background conditions with a mode radius of 80 nm and a mode width of 1.6. Relative extinction error is shown in the left panel with the relative mode radius error shown on the right.
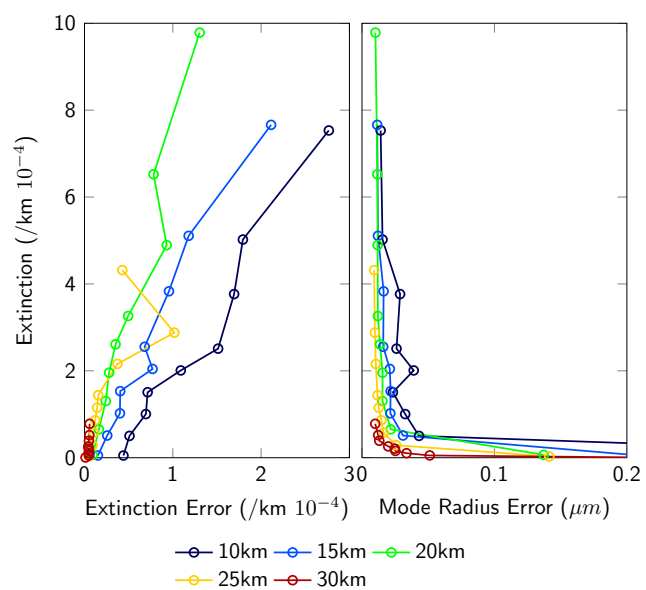
Fig. 7. Error in the retrieved extinction and mode radius parameters due to measurement noise as a function of extinction and tangent altitude. This was calculated by retrieving the error of a typical forward scatter geometry with varying amounts of aerosol loading.
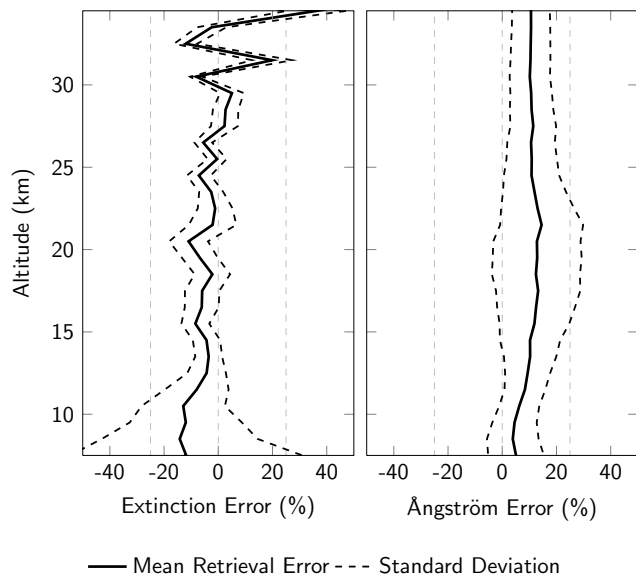
Fig. 8. Error in the retrieved parameters under a variety of simulated measurement conditions when the true atmospheric state is bimodal. Error using the coupled extinction and mode radius retrieval are shown in black with dashed lines showing the standard deviation.
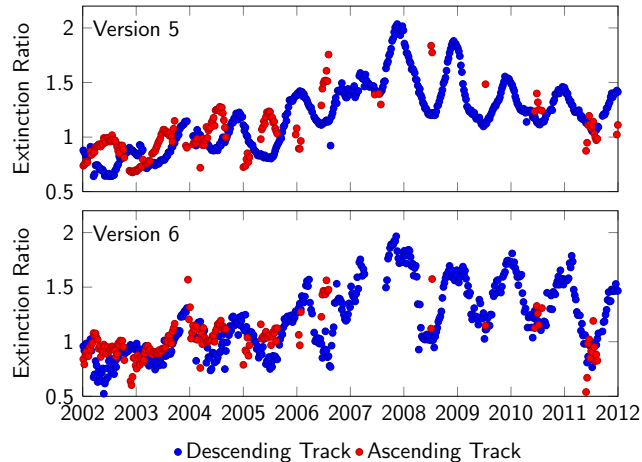
Fig. 9. Weekly averaged extinction ratio between 23 and 28 km from latitudes 20° N to 20° S split into the ascending (red) and descending tracks (blue). Results from the Version 5 retrieval are shown in the top panel with the results from the coupled particle size retrieval, denoted Version 6, shown in the bottom panel.
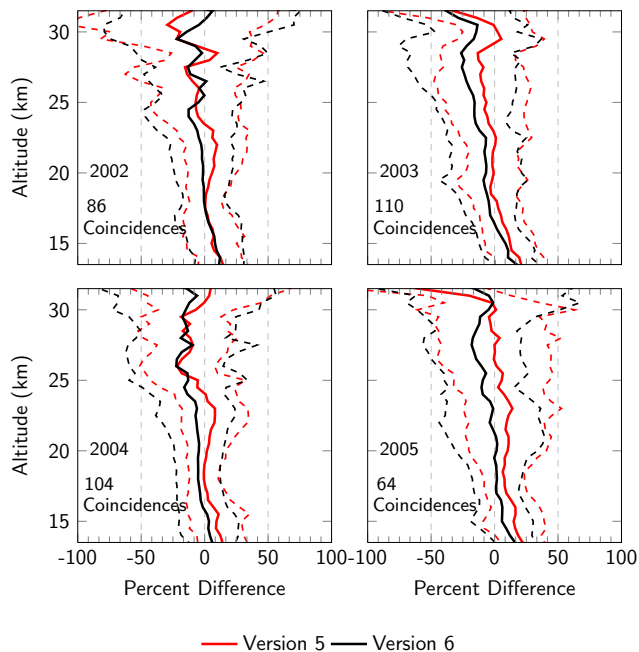
Fig. 10. Comparison of coincident SAGE III 755 nm aerosol extinction and OSIRIS 750 nm aerosol extinction. Each panel shows one year of coincident comparisons with the number of coincident profiles indicated in the respective panel. Mean percent differences are shown as solid lines with standard deviation shown as dashed. Version 5 retrievals are shown in red with Version 6 shown in black.

Title Page

Abstract | Introduction

Conclusions | References

Tables | Figures

◄ | ►|

◄ | ►

Back | Close

Full Screen / Esc

Printer-friendly Version

Interactive Discussion
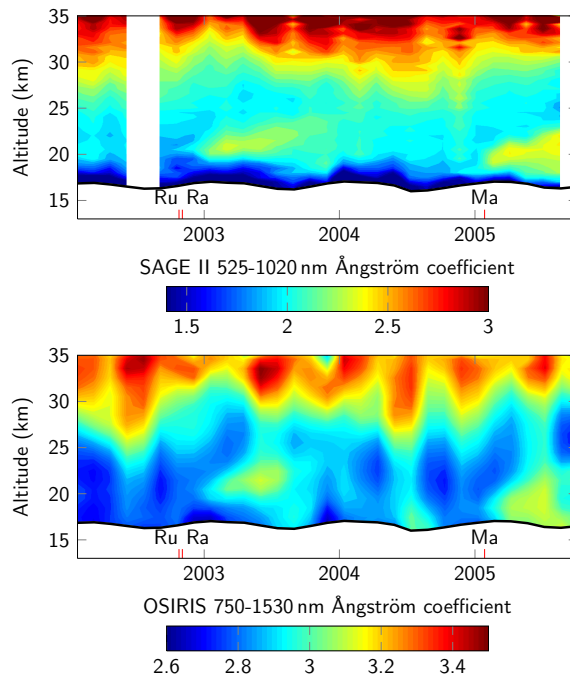
Fig. 11. Comparison of the OSIRIS and SAGE II Ångström coefficients. Top panel shows the SAGE II Ångström coefficient for 20° N to 20° S in 45 day averages, calculated from the 525 and 1020 nm channels. The bottom panel shows the OSIRIS Ångström coefficient for 20° N to 20° S in 45 day averages, using the coupled retrieval. Tropopause is denoted by the black line.